Sensitivity of megavoltage photon beam Monte Carlo simulations to electron beam and other parameters

Daryoush Sheikh-Bagheri[a] and D. W. O. Rogers[b]
Ionizing Radiation Standards, National Research Council of Canada, Ottawa, Ontario K1A 0R6, Canada

(Received 21 May 2001; accepted for publication 21 November 2001; published 21 February 2002)

The BEAM code is used to simulate nine photon beams from three major manufacturers of medical linear accelerators (Varian, Elekta, and Siemens), to derive and evaluate estimates for the parameters of the electron beam incident on the target, and to study the effects of some mechanical parameters like target width, primary collimator opening, flattening filter material and density. The mean energy and the FWHM of the incident electron beam intensity distributions (assumed Gaussian and cylindrically symmetric) are derived by matching calculated percentage depth-dose curves past the depth of maximum dose (within 1% of maximum dose) and off-axis factors (within 2σ at 1% statistics or less) with measured data from the AAPM RTC TG-46 compilation. The off-axis factors are found to be very sensitive to the mean energy of the electron beam, the FWHM of its intensity distribution, its angle of incidence, the dimensions of the upper opening of the primary collimator, the material of the flattening filter and its density. The off-axis factors are relatively insensitive to the FWHM of the electron beam energy distribution, its divergence and the lateral dimensions of the target. The depth-dose curves are sensitive to the electron beam energy, and to its energy distribution, but they show no sensitivity to the FWHM of the electron beam intensity distribution. The electron beam incident energy can be estimated within 0.2 MeV when matching either the measured off-axis factors or the central-axis depth-dose curves when the calculated uncertainties are about 0.7% at the 1 σ level. The derived FWHM ($\pm$0.1 mm) of the electron beam intensity distributions all fall within 1 mm of the manufacturer specifications except in one case where the difference is 1.2 mm.
[DOI: 10.1118/1.1446109]

I. INTRODUCTION

The BEAM code system[1] is a general purpose EGS4[2] user-code for the simulation of radiotherapy beams, especially those from linear accelerators. The original work by some of the developers focused mainly on electron beams[3–6] but the code has been widely used to simulate photon beams as well.[7–22] In a recent paper[23] we have demonstrated that BEAM is capable of matching carefully measured photon beam dose distributions very accurately without "tuning" linac model parameters (within $\pm$0.5% of local dose on the central axis including build-up, and generally within 1 mm for profiles). The advantage of that study was that all dimensions and materials of the linac, as well as the incident electron beam energy and spatial intensity distributions were known independently and did not need to be derived from dose measurements. Furthermore, all the information about the linac could be shared so others could verify the calculations independently. The situation for radiotherapy linacs is not as ideal since linac specifications are sometimes hard to get, especially due to the proprietary nature of the information. In addition to this, these specifications, although generally accurate, may be subject to user misinterpretations, undocumented linac updates and large uncertainties in the most important parameters needed for the simulation: in particular, the electron beam energy and intensity distributions. Some manufacturers have made praiseworthy efforts to provide, in easily accessible form and in considerable detail, the data needed for Monte Carlo simulations.[24]

Other techniques have been used to derive photon beam spectra from depth-dose measurements,[25] but now that Monte Carlo simulations are becoming increasingly useful in many aspects of radiotherapy, it makes sense to derive the parameters of the Monte Carlo linac simulations directly from measurements. To estimate the mean electron energy incident on the target, in-water dose profiles have been suggested as a more sensitive indicator than the depth-dose curve.[21,26] The flattening filter design causes the average energy and consequently the dose at depth to be relatively lower at off-axis points. This has been discussed by numerous authors.[27–35] The sensitivity of dose profiles as a measure of the electron beam parameters, however, is reduced with depth since phantom scatter becomes more prevalent. Since profiles are most sensitive to the incident beam characteristics if they are measured in-air and not in a phantom, in-air off-axis factors are used in this study.

The primary goal of this work is to develop a technique to derive best estimates for the energy and intensity distributions of the incident electron beam and apply this technique to nine beams from Varian, Elekta, and Siemens linacs to demonstrate its viability. This is done by comparing calculated and measured values of in-air off-axis factors for large fields (defined below) and central-axis relative depth-dose curves for $10\times10\ \mathrm{cm}^2$ fields. In Sec. II we also use in-air off-axis factors to study the sensitivity of our linac models to various parameters, including, but not limited to, variations in the incident electron beam, primary collimator, and flattening filter specifications. These parameters are not directly derivable from measurements and every effort must be made to specify them as accurately as possible before the onset of the simulations.

This work assumes the existence of a ''generic'' linac for each beam simulated, since both the linac specifications and the measured data used in this work are more or less generic. However, assuming one has reliable data for both the linac specifications and the dose measurements for an individual machine, our method is equally applicable. Most of the ''measured data'' in this paper come from the AAPM's TG-46 compilation of average depth-dose and off-axis factor measurements for various numbers of linacs.[36] Large error bars on a given piece of data indicates substantial variation in the values included in the compilation. For Elekta (Philips) machines the data published by Palta *et al.*[37] are used since, unlike TG-46,[36] they include the build-up region. TG-46[36] compares its compiled relative depth-dose data with those of Palta[37] past depth of maximum dose and the data agree to better than 0.8% for a $10\times 10\ \mathrm{cm}^2$ field. Due to the lack of relative depth-dose data for the Siemens KD machine at 18 MV in the TG-46[36] compilation, careful measurements for this beam, performed by Siemens scientists (Dr. Alf Siochi, personal communication), are used. In all cases, the relative depth-dose data are assumed to be measured and corrected properly according to dosimetry protocols, although this is not known for certain. For example, accurate measurements of the relative depth-ionization are expected to account for the effective point of measurement of the ion chamber and the variation of $(\overline{L}/\rho)^{\mathrm{water}}_{\mathrm{air}}$ with depth.[23]

For matching of the incident electron beam energy and intensity distribution, one advantage of using in-air off-axis factors is that they can be calculated faster (i.e., no phantom simulation is necessary), and are not sensitive to the exact shape of the electron-beam energy distribution. However, they are very strongly dependent on *both* the electron beam energy and radial intensity distributions, so off-axis factors cannot be used alone. Manufacturers usually specify that the electron-beam radial intensity distribution is Gaussian shaped and measurements confirm this on the NRC research linac.[23] Therefore, it is the FWHM of the Gaussian that is varied when the radial intensity distribution of the electron beam is adjusted in the simulations. The advantage of comparing relative depth-dose values is that they are strongly related to the electron beam energy but not to its radial intensity distribution. However, they are also somewhat sensitive to the electron-beam energy distribution. We use both in-air off-axis factors and central-axis depth-dose curves to lead to a consistent set of estimates for the incident electron beam energy and intensity distributions.

It is an iterative process to determine a consistent set of simulation parameters (i.e., electron beam energy and radial distribution of the incident beam). First, the simulation is run by starting with the manufacturer's specifications or suggestions for these parameters. Assuming that this does not lead to a satisfactory match of the off-axis factors or central-axis relative depth-dose values, one then adjusts the incident electron mean energy to match the depth-dose curve. Once this is matched, the radius of the incident radial distribution is varied to get a match with the in-air off-axis factors. If a match cannot be achieved, it may be necessary to re-adjust the mean energy somewhat to achieve agreement with the in-air off-axis factors. Once this agreement is satisfactory, it is essential to verify that the central-axis depth-dose curve is still matched adequately since the incident mean energy has been changed.

Sections II and III describe how the off-axis factors and relative depth-dose values are calculated and compared with measurements and what factors they are most sensitive to.

II. MATCHING IN-AIR OFF-AXIS FACTORS

A. In-air off-axis factors

The in-air off-axis factor at a distance x_j from the central axis, is defined as the ratio of dose-to-water at that point to the dose-to-water on the central axis, at a given SSD (usually 100 cm). The in-air off-axis factors are measured with an ion chamber with a full build-up cap or miniphantom to approximate charged-particle equilibrium (CPE). By ignoring wall attenuation and any change in ion chamber response per unit dose across the field due to variations in beam quality, the ion chamber reading can be taken as the in-air off-axis factor. To avoid a separate (CPU-intensive) Monte Carlo simulation of an ion chamber, the off-axis factors are approximated here using the water-kerma-weighted photon fluence (defined below). In the Monte Carlo calculations the water-kerma-weighted photon fluence (y_j) is scored in 15 annular bins, uniformly ranging from 0 to 35 cm. The off-axis factor in the jth radial bin, OAF_j, is defined as

$$\mathrm{OAF}_j = \frac{y_j}{y_1}. \tag{1}$$

The uncertainties in OAF_j are assessed by doing the calculations in 20 batches (on 20 machines) and taking the standard rms deviation on the mean. The uncertainty in the central bin is added (in quadrature) to the uncertainty of the subsequent bins to account for the effect of normalization of off-axis factors to the central bin. Consequently the central bin is assigned an uncertainty of zero.

To avoid binning artifacts, water kerma is calculated by weighting each photon reaching the scoring plane by the product of its energy, the mass energy-absorption coefficient for water calculated at that energy, and one over the cosine of the angle it makes with the z-axis. The mass energy-absorption coefficient for water is obtained from linear interpolation of data from Hubbell and Seltzer.[38] Assuming the fluence is constant over the central bin, the content of the first bin, y_1, is assigned to $x_1 = 0$, but for all the other bins the x_j represent the *center* of the jth bin.

B. Computational considerations

The off-axis factor calculations required between 5×10^5 (25 MV) and 5×10^6 (4 MV) initial electron histories, to obtain better than 1% uncertainty in the first bin ($0 \leqslant r \leqslant 2.33$ cm). At 4 MV the linac simulation ran at 4.5×10^5 histories/hour on a 200 MHz Pentium Pro PC. For the 25 MV simulation this number was 4.7×10^4 histories/hour. The selective bremsstrahlung splitting parameters[10,39] for the off-axis factor simulations are as follows: The maximum splitting factor (N_{max}) is 400, the minimum splitting factor (N_{min}) is 40, and the field radius (R_f), needed to calculate the probability of photon emission into the field, is 50. Additionally, in all of the off-axis factor simulations, Russian Roulette is played on the electrons and the positrons set in motion by split photons. Russian Roulette eliminates, in a random fashion and on average, all but one of the electrons or positrons set in motion by split photons of one group, readjusting the weight of the surviving electron or positron to that of the original electron that created the group of photons through the splitting routine.

The relative depth-dose calculations use the BEAM code's CHAMBER component module since it has an efficient range rejection technique. The water phantom has a radius of 25 cm, is 50 cm deep and is divided into variable-thickness depth slices, with 2 mm thick slices around the depth of maximum dose. Dose is calculated in the central region of the phantom which has a radius of 1 cm. The dose calculations are also processed in parallel and result in 20 separate sets of dose distribution files, where each set consists of up to 10 dose component files based on the LATCH bits assigned to the corresponding component module. When all the distributed calculations are finished, the results are combined into one set of (up to) 10 dose component files, but the main components used in this work are the total dose and the electron contamination dose. The splitting parameters for all linac simulations needed to calculate relative depth-dose curves (for a 10×10 cm^2 field), are $N_{\mathrm{max}}=400$, $N_{\mathrm{min}}=40$, $R_f=30$, and Russian Roulette is switched off, since in the case of dose calculations one is interested in good statistics for both photons and electrons. No photon interaction forcing is used. The values of the electron (ECUT) and the photon (PCUT) transport cutoff energies in all the simulations are 0.700 and 0.010 MeV, respectively. Range rejection is turned on with an ESAVE value of 0.7 MeV in the target for all beams and a value of 1.0 MeV in the rest of the linac for the 4 MV simulations and a value of 2.0 MeV for all the higher-energy beams. These cutoffs provide the largest saving in CPU time while preserving an accurate simulation. This is based on a range-rejection study which showed that the amount of bremsstrahlung that was ignored as a result of range-rejection, was less that 0.2% of total fluence. This study was done by tagging bremsstrahlung photons that are produced anywhere in the linac except in the target.

The linac simulations (all for 10×10 cm^2 fields) ran between 3.1×10^5 histories/hour at 4 MV, and 2.8×10^4 histories/hour at 25 MV. A total of 3.2×10^7 and 2×10^6 electron histories are run for the 4 and 25 MV linac simulations, respectively. The total number of particle records in the 20 phase-space files (and therefore not restricted to the actual field) is 4.52×10^6 photon records and 20 000 electron and positron records at 4 MV, and 5.04×10^6 photon records and 72 000 electron and positron records at 25 MV. The subsequent 20 dose calculations read a total of 4×10^8 (4 MV) and 2×10^8 (25 MV) entries from the corresponding phase-space file, recycling the phase-space files 80–90 times. Due to the enormous cycle length[40] of the random number generator (2^{144}), the small number of random numbers (of the order of thousands) needed to simulate a complete photon history and the spatial spread of photon interactions in the phantom, it is acceptable to recycle the phase-space in this manner. However, if the phase-space under-samples the actual underlying physical distributions, then recycling will lead to biased results. For example, if the spectrum of photons incident on the phantom is missing high-energy photons, then no matter how often the phase-space is recycled, it will not lead to the right dose distribution. Therefore the statistics of the phase-space must be good enough to represent all classes of particles (e.g., photons vs electrons, or scatter vs direct). Basically, the statistical uncertainty one can achieve in the dose calculation cannot be better than the statistical uncertainty in the underlying phase-space. In the phase-space files corresponding to the 10×10 cm^2 field linac simulations, the uncertainty in the photon fluence on the central axis (in the first radial bin, $0 \leqslant r \leqslant 2.25$ cm) is around 0.2%. The dose calculation ran at 1.26×10^7 histories/hour at 4 MV, and 1.11×10^7 histories/hour at 25 MV.

C. Sensitivity to the mean energy of the e^- beam

The off-axis factors are very sensitive to the mean energy of the electron beam. Hence they are used along with relative depth-dose data to derive the energy of the electron beam incident on the target. Manufacturers usually state that their specified energies for the incident electron beams are only starting points for the Monte Carlo simulations and therefore are only recommendations. Additionally, these recommendations can be subject to revisions (see Table I). Furthermore, tuning of the linac can change the energy of the electron beam incident on the target in a specific machine, and subsequently the user needs to quantify the energy being used. Here, our derived values correspond to those of an ''average'' linac. Figure 1 shows a series of off-axis factor calculations performed (for a Siemens KD 6 MV beam) when the incident electron beam energy is varied in steps of 0.1 MeV. The value of off-axis factor at 15 cm is selected from the calculations shown in Fig. 1 and plotted against energy of the incident electron beam, as shown by the inset. The relationship is linear and the off-axis factor at 15 cm radius for this beam drops as the energy of the beam is increased. The drop results from a combination of (a) the decrease with increasing energy in the mass scattering power (a measure of the angular deflection of the electron per unit mass thickness); (b) the increased transmission through the central part of the flattening filter due to beam hardening, and (c) the narrowing of the angular distribution of bremsstrahlung photons as the energy of the electron is increased. The combination of these factors reduces the horns as the energy increases.

TABLE I. Characteristics of the electron beams used in the photon beams studied in this work. E_e is the mean energy of the electron beam incident on the target. Both the distribution of the electron energy and the electron radial intensity are assumed Gaussian in shape. The energy spread is given at FWHM. In this work both the off-axis factors and the central-axis relative depth-dose values are used to derive the electron beam mean energy and the FWHM of its radial intensity distribution. Note that the electron beam energy spread is not derived but taken as that nominally specified by the manufacturers. The modeled electron beams are incident normal to the target and have no divergence. The uncertainty of the derived energies is about ±0.15 MeV and that of the derived FWHM is about ±0.01 cm.

Linac	Nominal potential (MV)	Nominal E_e and spread MeV	Derived E_e MeV	Nominal e^- beam FWHM (cm)	Derived e^- beam FWHM (cm)
Varian Clinac low-energy	4	4 (3%)	3.7	0.1	0.15
Varian Clinac high-energy	6	6 (3%)	5.7	0.1	0.2
	10	10 (3%)	10.5	0.1	0.15
	15	15 (3%)	14.5	0.1	0.17
	18	18 (3%)	18.3	0.1	0.11
Elekta SL25	6	6 (17%)	6.3	0.1	0.11
	25	19 (5%)	19.0	0.1	0.10
Siemens KD	6	5.52 (14%)[a]	6.8	0.2	0.32
	18	12.87 (14%)[b]	14.7	0.2	0.10

[a]New revised value by the manufacturer: 6.6 MeV.
[b]New revised value by the manufacturer: 14.68 MeV.

The energy resolution provided by comparing off-axis factors is about 0.2 MeV (see inset in Fig. 1) when the uncertainty in the off-axis factor at each point is about 0.7% (1 σ). This means that, as a rule of thumb, there has to be approximately a 0.2 MeV change in the incident electron energy, to see an observable change (2% or 3 σ with 0.7% statistics) in the off-axis factor for the range of energies studied here.

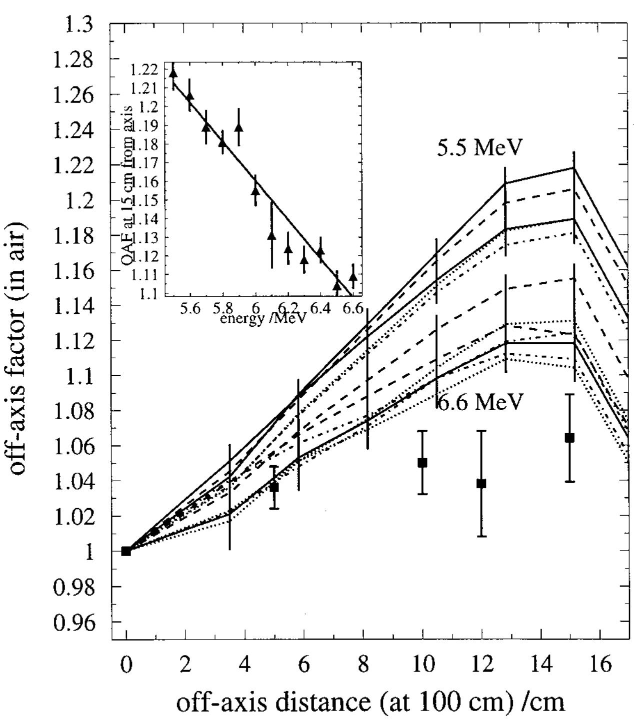

FIG. 1. An energy sensitivity study at 6 MeV for a Siemens KD machine. The energy of the incident electron beam is varied from 5.5 to 6.6 MeV in steps of 0.1 MeV, with an energy spread of 1% at FWHM. The off-axis factors at 15 cm are plotted vs the energy of the incident electron beam in the inset. The data are fit to a straight line of slope $-0.105 \pm 0.007\ \mathrm{MeV}^{-1}$. The filled squares are measured data from TG-46 (Ref. 36). The derived energy in this case is 6.8 MeV.

D. Sensitivity to the energy distribution of the e^- beam

As in the case of the electron-beam mean energy and intensity distribution, manufacturers' specifications for the electron-beam energy distribution (see Table I) can only be taken as a first estimate.

Since the off-axis factors are very sensitive to the mean energy of the electron beam, one might expect the actual width of the energy distribution of the electron beam to be important too. Figure 2 shows that as the FWHM of the electron-beam energy distribution for a 6 MV beam of a Siemens KD machine is varied from 0 to 20%, no correlation is observed within statistical uncertainties between the off-axis factors and the electron beam energy spread. The figure shows that (for a practically symmetric electron energy distribution) the effects of multiple scattering and Bremsstrahlung angular distribution for electrons of energy higher than the mean, are compensated by those for electrons with energy lower than the mean, leaving the final photon distribution similar to that emitted by monoenergetic electrons having the mean energy.

However, this can only be true if the electron energy distribution is fully symmetric and if only first order effects are considered. In general, due to the nonlinear variation of attenuation and scattering with energy, some differences should be observable. For example, the relative depth-dose values show a weak sensitivity to the electron beam energy spread, especially at larger depths.

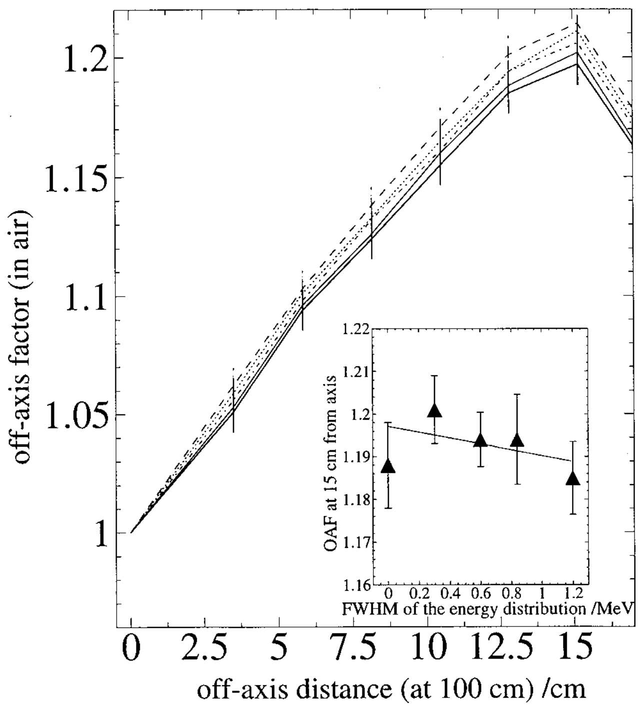

FIG. 2. Variation of off-axis factors at 6 MV (6 MeV peak intensity), as the energy spread of the electron beam incident on the target is varied from monoenergetic (thick solid line) to 5% (dashed line), 10% (dotted line), 14% (dashed–dotted line), and 20% (thin-solid line) energy spread at FWHM. The inset shows the values of off-axis factor at 15 cm plotted versus the FWHM of the energy distribution and the solid line is a fit with a slope of -0.008 ± 0.01: no significant correlation is observed at the 0.7% (1σ) level. The apparent correlation as a function of off-axis distance is an artifact of normalizing data to the central axis value.

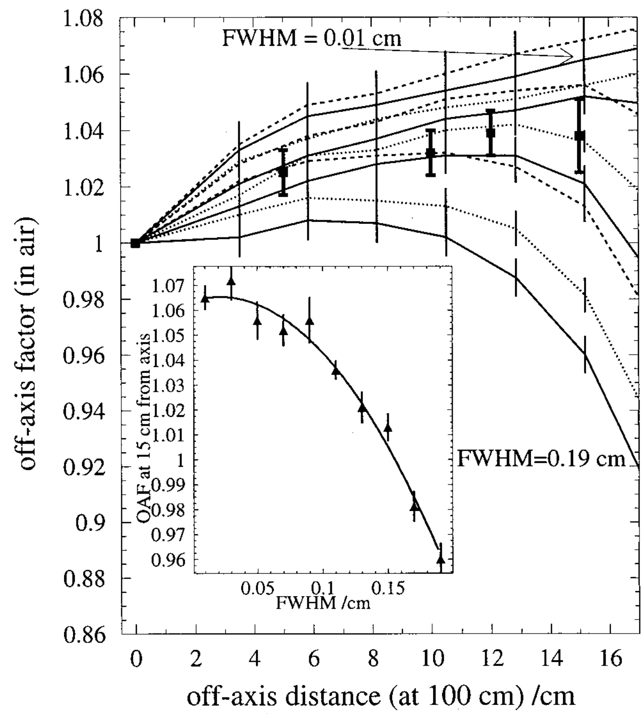

FIG. 3. Comparison of the calculated off-axis factors with measurements at 18 MV for a Varian machine, as the FWHM of the electron beam intensity distribution is varied between 0.01 cm and 0.19 cm, in steps of 0.02 cm. The inset shows the off-axis factors at 15 cm vs the FWHM of the radial intensity distribution of the electron beam incident on the target. The solid curve in the inset shows a quadratic fit to the calculations. The filled squares are measured data from TG-46 (Ref. 36).

Since these sensitivities are not large enough to be conclusive, the electron beam energy spread is modelled as specified by the manufacturers. For the 18 MV beam of the Siemens KD machine, the manufacturer suggests that the energy distribution is not a Gaussian and instead it is more like a Lorentzian with a sharper fall off past the peak. This energy distribution is approximated by adjoining two half-Gaussian distributions with the FWHM of the low-energy side taken as 14% (of the electron energy distribution peak) and that of the high-energy side taken to be 3%. Modeling this asymmetrical energy distribution results in a difference in the calculated off-axis factors at 15 cm off axis of about 2% as indicated by the dotted line in the Siemens KD 18 MV panel of Fig. 8 which is presented below.

E. Sensitivity to the radial intensity distribution of the e^- beam

The electron-beam radial intensity distribution influences the off-axis factors to a great extent. Generally speaking, the larger the width of the electron-beam radial intensity distribution, the relatively more intense the photon beam on the central axis. The central-axis relative depth-dose values, on the other hand, are quite insensitive to such variations in the electron beam intensity distribution, because the shape of the central-axis relative depth-dose, (ignoring the e^- contamination), is primarily determined by those photons which are incident on the phantom around the central axis itself.

As in the case of the electron beam energy, most manufacturers do not provide an accurate description of the electron beam radial intensity distribution. It is generally recommended that the electron beam intensity distribution be taken as Gaussian with a FWHM of around 0.1 cm (see Table I). Figure 3 shows (for the 18 MV beam of a Varian linac) a series of calculated off-axis factors for a series of Gaussian electron beams with the FWHM of the beam's radial intensity distributions varied from 0.01 cm to 0.19 cm in steps of 0.02 cm. To quantify the dependence of off-axis factors on the FWHM of the intensity distribution of the electron beam, the values of off-axis factor at 15 cm are plotted versus FWHM and displayed by the inset in Fig. 3 which shows that the off-axis factor drops quadratically with increasing FWHM of the electron-beam radial intensity distribution.

F. Sensitivity to the divergence of the e^- beam

Since the electron beam radial intensity distribution has an important effect on the off-axis factors, one would expect the electron beam divergence to play a role also. The divergence of the electron beam is initially modeled as a smoothly varying function of the radial position of the electron with respect to the central axis and it is specified at half-width at half maximum of the electron radial intensity distribution.

To study the effect of divergence on the off-axis factors, for an electron beam with an intensity distribution FWHM of 0.1 cm, the divergence is varied from none to an angle of 1° (corresponding to being aimed nearly 2 cm off-axis at 100 cm). The divergence is quoted here at a radius of 0.05 cm from the axis of symmetry of the electron beam. Up to a divergence of 0.5°, and at 0.3% statistics level, no difference in the calculated off-axis factors is observed. When the divergence is set to 1°, the off-axis factor at 15 cm radius decreases by close to 1% for an 18 MV beam. The bremsstrahlung emitted by a more divergent electron beam is blocked more efficiently by the primary collimator, reducing the amount of scatter that reaches off-axis points and therefore could explain the behavior of off-axis factor when the divergence is increased.

Depth–dose curves have been shown to be insensitive to a divergence of even 5° at half-width at half maximum (0.05 cm) of the electron beam intensity distribution, for 1% statistics (1σ).

The divergence of the electron beam incident on the target is ignored in this work, since there is no reliable estimate provided by the manufacturers and since credible divergences of up to 0.5° show no observable effect.

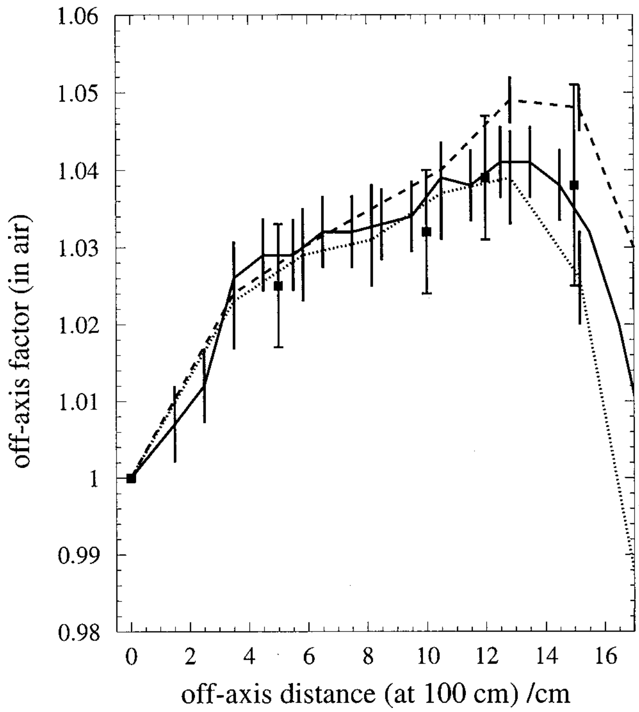

FIG. 4. The sensitivity of off-axis factors for an 18 MV Varian beam to a variation of 0.01 cm in the upstream radius of the primary collimator. The off-axis factors are calculated for the following selections of the upstream radius of the primary collimator; 0.226 cm (dotted line), 0.236 cm (solid line), and 0.246 cm (dashed line). The electron beam is modeled as a pencil beam of radius 1 mm. The filled squares are measured data from TG-46 (Ref. 36).

G. Sensitivity to the upstream opening of the primary collimator

The primary collimator is one of the components of the linac with a potential to influence off-axis factors. The details of the geometry of the primary collimator are much better known (and specified by the manufacturer) than, for example, the electron beam energy and intensity distribution. Therefore, the primary collimator geometry is not taken as a parameter in the simulations, and is only varied to show the size of its effect. This influence mostly occurs at the upstream opening of the primary collimator where the opening restricts the fluence of bremsstrahlung photons originating from the target that could contribute to the scattered photon fluence reaching off-axis points further downstream. For example, opening (or closing) the primary collimator's upstream opening by 0.01 cm (i.e., by changing the opening angle) for an opening radius of 0.246 cm and an electron beam radius (pencil beam) of 0.1 cm, results in a 1% increase (or decrease) in the value of off-axis factor at 15 cm, in an 18 MV photon beam of a Varian linac (see Fig. 4).

Therefore, the exact opening of the primary collimator must be known to better than 0.01 cm when matching off-axis factors.

H. Sensitivity to material and density of the flattening filter

The manufacturers provide very precise dimensions of the flattening filter. However, our own experience showed problems with the initial specifications of the material and the density of the flattening filter. For example, for one machine the machine drawing specified copper as the material of the flattening filter. Since the density and therefore the material of the flattening filter strongly influences the off-axis factors, a comparison of the calculations to measured data excluded the possibility of the flattening filter being made of copper. Upon further communication with the manufacturer it became clear that the flattening filter was made of tungsten and that the machine drawing was in error. As an example, if the flattening filter is simulated as if made of Cu, Pb or W, the off-axis factor at 15 cm, calculated with the Cu-flattening filter ($\rho = 8.9$ g/cm^3) is 50% lower than that calculated assuming a W-flattening filter ($\rho = 19.3$ g/cm^3), and the corresponding value using a Pb-flattening filter ($\rho = 11.34$ g/cm^3) is 33% lower (see Fig. 5 showing results for a 15 MV beam).

This sensitivity is primarily due to differences in the density. Even a flattening filter of a certain material can have different densities depending on the manufacturing process used. For example, the density of different types of pure W varies by more than 1 g/cm^3 and if the density of the W-flattening filter is decreased by 1 g/cm^3, the calculated off-axis factor decreases by 6% at 15 cm radius (see Fig. 6 which shows results for the 15 MV beam of a Varian linac).

Therefore, any attempt to match off-axis factors must use accurate material densities, especially for the flattening filter.

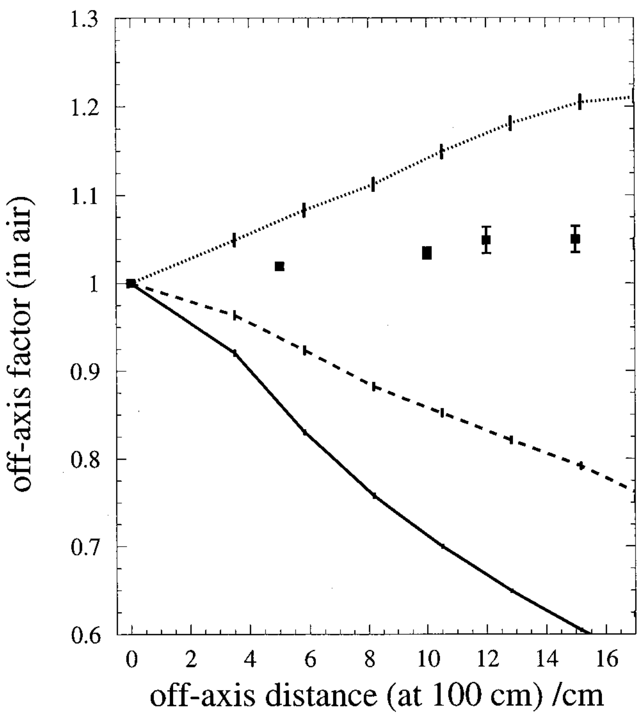

FIG. 5. The sensitivity of off-axis factors to the material of the flattening filter in a 15 MV Varian machine: Cu with a density of 8.933 g/cm^3 (solid line), Pb with a density of 11.34 g/cm^3 (dashed line), and W with a density of 19.30 g/cm^3 (dotted line). The filled squares are measured data.

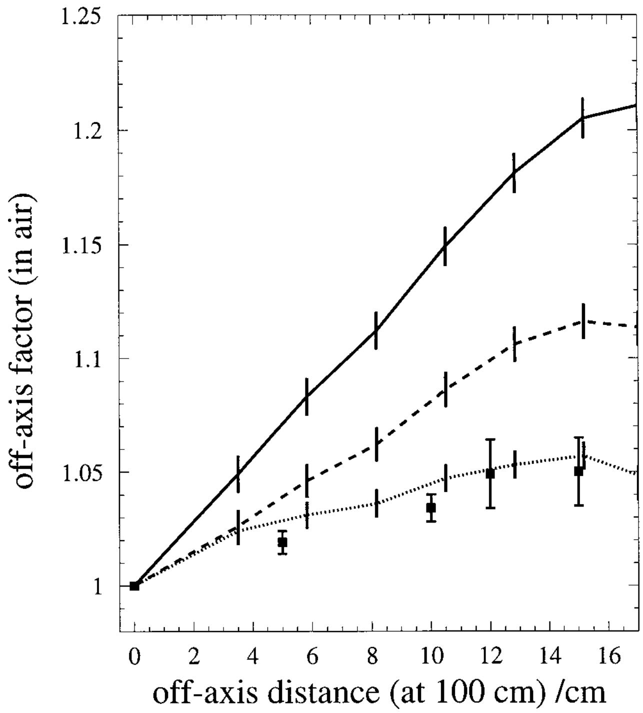

FIG. 6. The sensitivity of off-axis factors for a 15 MV Varian machine to the density of the W flattening filter, 19.3 g/cm^3 (solid line), 18 g/cm^3 (dashed line), 17 g/cm^3 (dotted line). The filled squares are measured data from TG-46 (Ref. 36).

I. Sensitivity to the angle of incidence of the electron beam

If the angle of a parallel beam of electrons incident from vacuum is changed from 0.0° to 0.5° (corresponding to being aimed 0.9 cm off-axis at 100 cm), the entire shape of the off-axis factor plot is changed (see Fig. 7 which shows results for the 18 MV beam of a Varian linac). Compared to normal incidence, the off-axis factors in the oblique case are higher by more than 1%, up to a radius of about 12 cm, but lower by about 4% at 15 cm.

Figure 7, however, does not represent the variation of measured off-axis factors, if the angle of incidence of the electron beam is changed in reality. The reason is that the calculated off-axis factors assume cylindrical symmetry and are scored in concentric annular regions around the central axis of the linac to improve statistics. The goal of this part of the sensitivity study is just to show that off-axis factors, even the way they are calculated in this work, are very sensitive to the angle of incidence of the electron beam on the target. In practice the assumption of normal incidence is a sound one, since non-normal incidence would strongly affect beam flatness and symmetry.

J. Sensitivity to the lateral dimensions of the target

Some manufacturers indicate that the target's lateral dimensions should have no observable effect on the simulations. Calculations are done for square targets with lateral width values of 20 cm, 3.2 cm, 2.0 cm, 1.0 cm, and 0.4 cm. In an 18 MV calculation where the primary collimator opening has a radius of 1.75 cm at a distance of 1.6 cm below the target face, we found that for a target width of 4 mm the off-axis factor was 8% low at 8 cm off-axis although for target widths of 1 cm or greater there were no statistically significant differences. Therefore, the target dimensions are not important as long as the target width is much larger than the lateral spread of electrons in the target or the radius of the upstream opening of the primary collimator. In the latter case, if the target's width is made too small, one misses scattered photons from within it and the calculated off-axis factors are reduced substantially.

K. Off-axis factors for all the beams studied

For all the beams studied here, Fig. 8 shows a comparison between the measurements and the off-axis factors calculated using the parameters specified in Table I. The calculated off-axis factors, for all beams studied, match those compiled by TG-46,[36] within uncertainties (2σ level). The calculated statistical uncertainties are typically 0.7%, at the 1 σ level. The uncertainties of the measured off-axis factors vary dramatically, since the number and variation in the data sets used in the TG-46[36] report varies for different beams.

The dashed lines in Fig. 8 show calculations done assuming the values specified by the manufacturers for the electron beam intensity distribution as shown in Table I. The additional dotted line in the Siemens KD 18 MV beam, represents calculations done assuming a FWHM of 14% for the energy distribution of the electron beam incident on the tar-

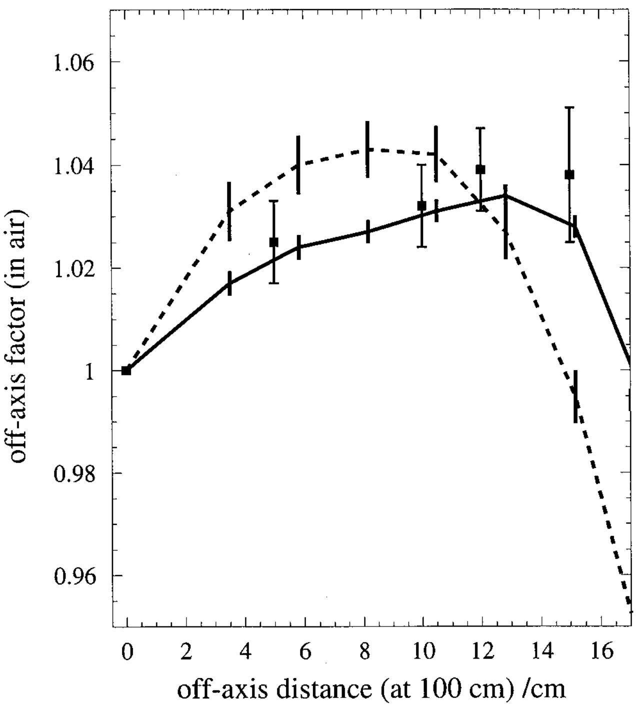

FIG. 7. The sensitivity of calculated off-axis factors to the angle of incidence of the electron beam on the target for an 18 MV Varian machine. Normal incidence (solid line), incidence at 0.5° to normal (dashed line). The electron beam used in this model is assumed to be monoenergetic with an energy of 18.6 MeV and a pencil beam with a radius of 1 mm. The filled squares are measured data from TG-46 (Ref. 36).

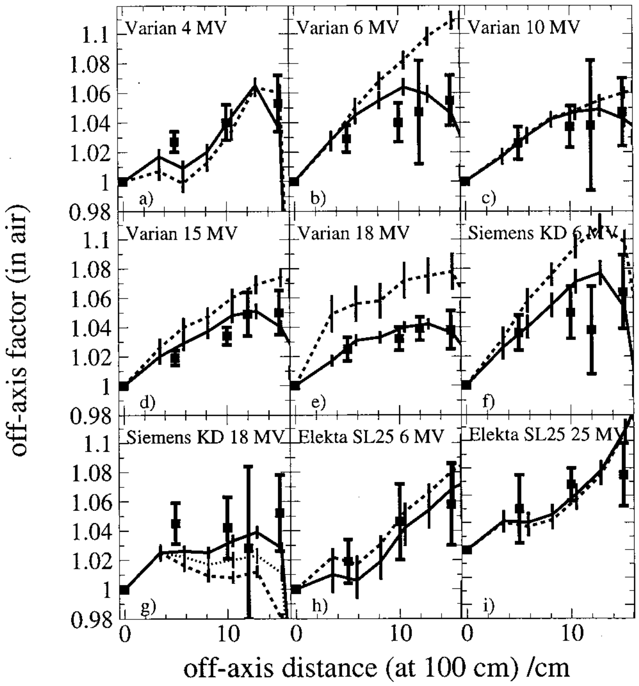

FIG. 8. Comparison of the calculated (solid lines) and measured (filled squares) [from TG-46 (Ref. 36)] in-air off-axis factors for open beams of 40×40 cm^2 for the linacs studied in this work. Because of the normalization at the center, the error estimate corresponding to the central bin is accounted for in the rest of the bins. The solid lines use the parameters derived for the corresponding electron beams as presented in Table I. The dashed lines use the nominal FWHM for the electron intensity distribution as specified by the manufacturer, but using our derived mean energies as used in the calculation of the solid lines. The dotted line in the Siemens KD 18 MV panel represents calculations assuming a Gaussian energy distribution (with a 14% FWHM) for the electron beam incident on the target.

get, as opposed to the solid line in the same panel which is calculated using an asymmetric energy distribution as discussed in Sec. II D.

III. MATCHING CENTRAL-AXIS DEPTH-DOSE DISTRIBUTIONS

As discussed before, matching off-axis factors alone does not lead to a uniquely specified beam energy, since in addition to the electron beam energy, the electron beam intensity distribution incident on the target also influences the off-axis factors (see Table I). Therefore more weight is given here to the determination of the electron beam energy obtained through matching of the central-axis depth-dose distributions.

Starting with the nominal radial distribution parameters the central-axis depth-dose curve is calculated for a 10×10 cm^2 field. The calculated values are then compared with the corresponding measurements compiled by TG-46.[36] If the calculated central-axis relative depth-dose values agree with measurements to better than 1.5% of local dose, for calculated uncertainties of 0.7% or less, then "a match" is found (see Fig. 9). The use of local dose difference instead of dose difference normalized to maximum dose, is a more sensitive measure of dose difference in the build-up region and especially at deeper depths. Using this method, variations in the energy of the electron beam of about 0.2 MeV produce observable (3σ) changes in the shape of the central-axis relative depth-dose curve, provided the uncertainty in dose at each point is about 0.7% ($1\ \sigma$) or better. If the agreement in the region past depth of maximum dose is worse than 2% (local dose), then the energy of the electron beam is varied until a match with the relative depth-dose values is obtained and then the off-axis factors are matched, mainly by adjusting the radial intensity distribution of the electron beam within a reasonable range.

Figure 9 shows the relative difference between the calculated depth-dose distributions (10×10 cm^2 fields) and the measurements for all the beams studied in this work. When comparing the simulations with the measurements, all data are normalized to the value of dose at 10 cm depth ($dd(10)$), which is obtained from a fourth order polynomial fit to the fall-off region of the depth-dose curve on the central axis (2 cm past depth of maximum dose down to a depth of about 21 cm). One could normalize the curves to maximum dose, but due to the relatively large statistical noise around depth of maximum dose, that method is not adopted in this work. The calculated depth-dose values are not converted to depth-ionization, since the measured data are reported as "dose," and the variation of $(\overline{L}/\rho)^{\mathrm{water}}_{\mathrm{air}}$ with depth makes only a small change in the shape of the depth-dose curve.[23] To provide a more sensitive comparison of calculated and

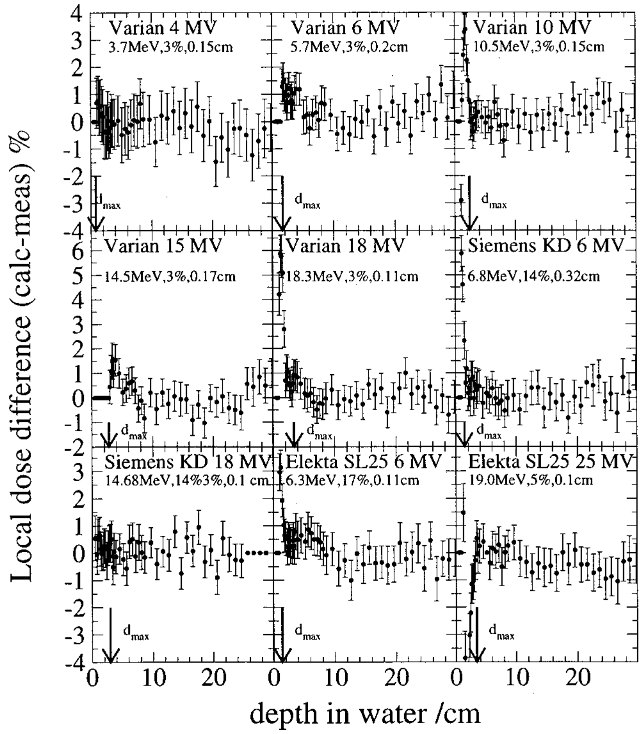

FIG. 9. Comparison of calculated and measured $\%dd$ values as local dose-difference plots for all the commercial linacs studied in this work. The values below the beam names are the peak intensity electron energy, the FWHM of the Gaussian energy distribution as a percentage of the peak intensity energy and the FWHM of the radial intensity distribution of the electron beam incident on the target, respectively. All measured data are from compilations of TG-46 (Ref. 36), except the two Elekta beams that are from Palta (Ref. 37) (since they include the build-up region) and the Siemens 18 MV beam which is provided by Siemens AG; (Dr. Alf Siochi, personal communication). Where no measured data were available the size of the error bars is set to zero. The field size is 10×10 cm^2 for all beams.

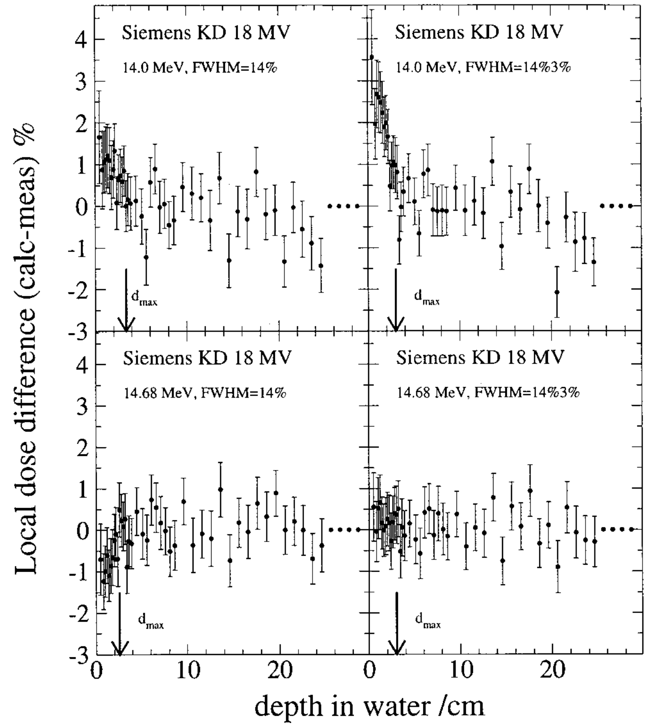

FIG. 10. Sensitivity of the calculated $\%dd$ values to the mean energy and the shape of the energy spectrum of the incident electrons on the target, for the 18 MV beam of the Siemens KD machine. The two panels on the right-hand side show calculations assuming an asymmetric width for the electron energy spectrum, as suggested by the manufacturer. The assumed FWHM = 14%3% means an asymmetric Gaussian with 14% FWHM on the LHS of the peak and 3% FWHM on the RHS of the peak.

measured depth-dose values, local-dose difference plots as shown in Fig. 9 are used.

The agreement in the build-up region, for those beams for which measured data in this region were available, has not been as good as the fall-off region of the relative depth-dose curve. No special attempt is made to improve the agreement in the build-up region, since the conditions under which the measurements, compiled by TG-46,[36] were performed (e.g., whether or not they were corrected for the effective point of measurement) are not exactly known. As shown elsewhere, the correction for the effective point of measurement makes a critical difference in the build-up region, when normalization is at a depth past depth of maximum dose.[23]

The availability of accurate measurements for the 18 MV beam of the Siemens KD machine made it possible to investigate the effects of the details of the electron beam energy distribution on the central-axis depth-dose distribution. Figure 10 displays the effect of modeling the asymmetry in the electron beam energy distribution (as suggested by the manufacturer), in comparison to the effect on the resulting depth–dose curves of changing the electron beam mean energy by 0.68 MeV. As seen by the two bottom panels, modeling the asymmetry in the electron beam energy distribution can affect the depth-dose distribution in the build-up region by as much as 1.5%.

IV. DISCUSSION

Table I summarizes the parameters found for the nine beams studied here. These are hard to compare to previous work since each study uses a different set of measured data as a starting point. Nonetheless, several general observations can be made.

The first comment concerns the incident energies that we assigned for the Siemens machines. These differed substantially from the manufacturer's original nominal values. After considerable discussion by ourselves and others modeling these machines,[14,22] it was found that Siemens had been providing the energy of the electrons incident on the target whereas modelers use the energy coming out of the accelerator vacuum. Faddegon *et al.* have demonstrated the sensitivity of the field flatness at 6 MV to both of the main parameters discussed here but they did not assign a final set of parameters.[14] Francescon *et al.* did the same and reported energies of 5.9 to 6.2 MeV and a beam radius of 1.1 mm.[22]

The Peregrine group has adopted a procedure which uses a fixed beam radius and adjusts the beam energy to match dose profiles at 10 cm depth.[21] As a result, they assigned an incident energy of 6.2 MeV for the Varian 6 MV beam compared to our value of 5.7 MeV. However, they use a nominal incident beam radius of 1 mm whereas we found a value of 2.0 ± 0.1 mm. Figure 1 (for a 6 MV Siemens beam) suggests that if we use 6.2 MeV instead of 5.7 MeV, then the in-air off-axis ratio would decrease by 5%. Figure 3 (and our less rigorous sensitivity study at 6 MV, not presented here) suggest that if we used a beam radius of 1 mm instead of 2 mm, the off-axis ratio would increase substantially (albeit, based on calculations for an 18 MV beam). Thus, by not adjusting the radius of the incident beam, the Peregrine group has assigned an incident energy which differs from ours by 9%. At 18 MV we found that the beam radius for the Varian machine was very close to the nominal beam radius of 1 mm which was also used by the Peregrine group. As a result our incident energy of 18.3 MeV is very close to theirs (18.5 MeV).

Several other studies have reported incident energies which tend to be higher than ours for the Varian machines (e.g., Liu *et al.*, 6.5 MeV for a Varian 6 MV beam[9] and Fix *et al.*, 6.05 MeV for the same beam[41]) but they provide little information about radial distributions of the incident beams.

It remains to be seen how important these differences are in clinical practice. Nonetheless, we believe that the procedure we have developed provides a consistent approach which accounts for our lack of detailed knowledge of two critical parameters of the incident electron beam.

V. SUMMARY AND CONCLUSIONS

The BEAM code, which was optimized[10] and benchmarked[23] previously, is used to simulate nine commercial medical linac beams from three major manufacturers. The linac simulations are performed using specifications representing ''generic'' linacs. The corresponding measurements are also generic in the sense that they are obtained by averaging data from different centres for the same beam.

To estimate the incident electron beam energy and intensity distribution, calculated off-axis factors and central-axis depth-dose curves are compared with measurements for each beam. The comparison with central-axis depth-dose data is used to specify the incident-electron mean-energy and show the sensitivity to its width. The in-air off-axis factors are then used to derive the FWHM of the electron beam intensity distribution. The electron beam radial intensity distribution (or its FWHM) influences the off-axis factors to a great extent. As the FWHM of the intensity distribution increases from zero to a few millimetres, the relative intensity of the photon beam on the central axis increases by a few percent. The central-axis relative depth-dose values, on the other hand, are quite insensitive to such variations in the electron beam intensity distribution.

No correlation is observed between the off-axis factors and the FWHM of an assumed Gaussian energy spread for the electron beam. The relative depth-dose values show some sensitivity to the electron beam energy spread, especially at larger depths. However the dependence is weak and therefore we use the widths supplied by the manufacturers. The derived FWHM of the electron radial intensity distributions are usually larger than those specified by the manufacturers (see Table I).

The divergence of the electron beam incident on the target in commercial linacs is ignored in the simulations because it was shown to have little effect,[23] it is not specified by the manufacturers and there is no practical method known to us to derive it from dose measurements.

Since, as expected, the calculations are very sensitive to the density of the flattening filter, it is important to get accurate values of this quantity from the manufacturers, especially for materials for which the density is known to vary depending on how it was manufactured.

The off-axis factors are shown to be very sensitive to the primary collimator upstream opening, as well as the flattening filter material and density, as expected. It is only possible to a limited extent, to check for variations in the density of materials using the methods presented here, therefore, it is recommended that the density of the flattening filter be known to better than 0.1 g/cm^3, to match off-axis factors accurately.

The calculated in-air off-axis factors, for all beams studied, match those compiled by TG-46,[36] within statistical uncertainties (at the 2 σ level). The calculated and measured depth-dose data agree within 1.5% (local dose), for 0.7% (1 σ level) statistics, at all depths past depth of maximum dose for all beams. The local-dose difference method used in this work (see Fig. 9) enhances the sensitivity of a relative depth-dose comparison appreciably. Using this method, the mean energy of the electron beam can be determined with a resolution of about 0.2 MeV when the uncertainty in dose at each point is about 0.7% (1 σ).

For two of the nine beams, the derived mean electron energy incident on the target were about 5% and 15% different from that originally specified by the manufacturer, but later the manufacturer revised the values and the new revised values are in agreement with our findings to 3% and 0%, respectively. For all the other beams the difference is less than 5%. The electron energy spread is taken as a Gaussian distribution with a FWHM based on manufacturers' data, since neither the off-axis factors nor the relative depth-dose values provide a sensitive enough tool to confidently derive this parameter. However, the 18 MV beam of the KD machine was the only beam specified by the manufacturer to have an asymmetric energy distribution with a sharper fall-off past the average energy, and therefore provided the opportunity to investigate the effect of the shape of the electron intensity distribution on the final depth dose curve (see Fig. 10).

This study provides a procedure for determining the two most important but often poorly specified parameters needed for simulating photon radiotherapy beams (viz. the mean energy and the FWHM of the intensity distribution of the incident electron beam). We have shown that it is possible to derive such parameters for generic machines but our method is equally applicable to individual machines, provided one has access to accurate dose measurements and information about the individual linac head.

ACKNOWLEDGMENTS

We would like to thank Varian, Siemens, and Elekta for providing us with the specifications needed for linac simulations. Our special thanks to Dr. Alf Siochi for his extensive sharing of knowledge regarding Siemens machines. One of the factors which made this work possible was prepublication access to TG-46 data, for which we thank Dr. Jim Purdy. We would also like to thank CERN for providing us with the PAW software and Dr. Michel Proulx of NRC for his help in computer network management and Blake Walters for support of the BEAM system. We wish to thank our colleagues Carl Ross and Ernesto Mainegra-Hing of NRC for helpful comments on the manuscript. This work was partially supported by NCI grant R01 CA52692 and by MDS Nordion.

[a]Ottawa Carleton Institute of Physics, Carleton University, Ottawa, ON. Present address: NOMOS Grp, www.nomos.com

[b]Electronic mail: dave@irs.phy.nrc.ca and WWW: http://www.irs.inms.nrc.ca/inms/irs/irs.html.

[1] D. W. O. Rogers, B. A. Faddegon, G. X. Ding, C. M. Ma, J. Wei, and T. R. Mackie, ''BEAM: A Monte Carlo code to simulate radiotherapy treatment units,'' Med. Phys. **22**, 503–524 (1995).

[2] W. R. Nelson, H. Hirayama, and D. W. O. Rogers, The EGS4 Code System, Report SLAC-265, Stanford Linear Accelerator Center, Stanford, California, 1985.

[3] G. X. Ding, D. W. O. Rogers, and T. R. Mackie, ''Calculation of stopping-power ratios using realistic clinical electron beams,'' Med. Phys. **22**, 489–501 (1995).

[4] G. X. Ding, D. W. O. Rogers, and T. R. Mackie, ''Mean energy, energy-range relationship and depth-scaling factors for clinical electron beams,'' Med. Phys. **23**, 361–376 (1996).

[5] G. G. Zhang, D. W. O. Rogers, J. E. Cygler, and T. R. Mackie, ''Effects of changes in stopping-power ratios with field size on electron beam ROFs,'' Med. Phys. **25**, 1711–1724 (1998).

[6] G. G. Zhang, D. W. O. Rogers, J. E. Cygler, and T. R. Mackie, ''Monte Carlo investigation of electron beam output factors vs size of square cutout,'' Med. Phys. **26**, 743–750 (1999).

[7] H. H. Liu, T. R. Mackie, and E. C. McCullough, ''Calculating output factors for photon beam radiotherapy using a convolution/superposition method based on a dual source photon beam model,'' Med. Phys. **24**, 1975–1985 (1997).

[8] H. H. Liu, T. R. Mackie, and E. C. McCullough, ''Calculating dose and output factors for wedged photon radiotherapy fields using a convolution/superposition method,'' Med. Phys. **24**, 1714–1728 (1997).

[9] H. H. Liu, T. R. Mackie, and E. C. McCullough, ''A dual source photon beam model used in convolution/superposition dose calculations for clinical megavoltage x-ray beams,'' Med. Phys. **24**, 1960–1974 (1997).

[10] D. Sheikh-Bagheri, Ph.D. thesis, Carleton University, Ottawa, 1999.

[11] K. M. Ayyangar and S. B. Jiang, ''Do we need Monte Carlo treatment planning for linac based radiosurgery? A case study,'' Med. Dosim **23**, 161–168 (1998).

[12] W. van der Zee and J. Welleweerd, ''Calculating photon beam characteristics with Monte Carlo techniques,'' Med. Phys. **26**, 1883–1892 (1999).

[13] C.-M. Ma, E. Mok, A. Kapur, T. Pawlicki, D. Findley, S. Brain, and K. Forster, ''Clinical implementation of a Monte Carlo treatment planning system,'' Med. Phys. **26**, 2133–2143 (1999).

[14] B. A. Faddegon, P. O'Brien, and D. L. D. Mason, ''The flatness of Siemens linear accelerator x-ray fields,'' Med. Phys. **26**, 220–228 (1999).

[15] J. V. Siebers, P. J. Keall, B. Libby, and R. Mohan, ''Comparison of EGS4 and MCNP4b Monte Carlo codes for generation of photon phase space distributions for a Varian 2100C,'' Phys. Med. Biol. **44**, 3009–3026 (1999).

[16] A. Schach von Wittenau, L. J. Cox, P. M. Bergstrom, W. P. Chandler, C. L. Hartmann-Siantar, and R. Mohan, ''Correlated histogram representation of Monte Carlo derived medical accelerator photon-output phase space,'' Med. Phys. **26**, 1196–1211 (1999).

[17] P. J. Keall, J. V. Siebers, R. Jeraj, and R. Mohan, ''The effect of dose calculation uncertainty on the evaluation of radiotherapy plans,'' Med. Phys. **27**, 478–484 (2000).

[18] K. Ayyangar, R. Mooij, and P. Nizin, OMEGA Monte Carlo verification of dosimetric data for gamma knife, in *The Use of Computers in Radiotherapy, XIIIth International Conference, Heidelberg*, edited by W. Schlegel and T. Bortfeld (Springer-Verlag, Heidelberg, 2000), pp. 464–465.

[19] J. V. Siebers, P. J. Keall, J. O. Kim, and R. Mohan, Performance benchmarks of the MCV Monte Carlo system, in *The Use of Computers in Radiotherapy, XIIIth International Conference, Heidelberg*, edited by W. Schlegel and T. Bortfeld (Springer-Verlag, Heidelberg, 2000), pp. 129–131.

[20] A. Schach von Wittenau, P. M. Bergstrom, and L. J. Cox, ''Patient-dependent beam-modifier physics in Monte Carlo photon dose calculations,'' Med. Phys. **27**, 935–947 (2000).

[21] C. L. Hartmann Siantar *et al.*, ''Description and dosimetric verification of the PEREGRINE Monte Carlo dose calculation system for photon beams incident on a water phantom,'' Med. Phys. **28**, 1322–1337 (2001).

[22] P. Francescon, C. Cavedon, S. Reccanello, and S. Cora, ''Photon dose calculation of a three-dimensional treatment planning system compared to the Monte Carlo code BEAM,'' Med. Phys. **27**, 1579–1587 (2000).

[23] D. Sheikh-Bagheri, D. W. O. Rogers, C. K. Ross, and J. P. Seuntjens, ''Comparison of measured and Monte Carlo calculated dose distributions from the NRC linac,'' Med. Phys. **27**, 2256–2266 (2000).

[24] R. A. C. Siochi, Requirements for Manufacturer Supplied Data for Monte Carlo Simulation: A BEAM Perspective, *Proceedings of the Fifteenth International Conference on the Applications of Accelerators in Research and Industry* (The American Institute of Physics, New York, 1999), pp. 1060–1065.

[25] A. Ahnesjo and P. Andreo, ''Determination of effective bremsstrahlung spectra and electron contamination for photon dose calculations,'' Phys. Med. Biol. **34**, 1451–1464 (1989).

[26] D. M. J. Lovelock, C. S. Chui, and R. Mohan, ''A Monte Carlo model of photon beams used in radiation therapy,'' Med. Phys. **22**, 1387–1394 (1995).

[27] W. F. Hanson, L. W. Berkley, and M. Peterson, ''Calculative technique to correct for the change in linear accelerator beam energy at off-axis points,'' Med. Phys. **7**, 147–150 (1980).

[28] A. G. Kepka, P. M. Johnson, and J. David, ''The effect of off-axis quality changes on zero area TAR for megavoltage beams,'' Phys. Med. Biol. **30**, 589–595 (1985).

[29] B. E. Bjärngard and H. Shackford, ''Attenuation in high-energy x-ray beams,'' Med. Phys. **21**, 1069–1073 (1994).

[30] F. M. Khan, B. J. Gerbi, and F. C. Deibel, ''Dosimetry of asymmetric x-ray collimators,'' Med. Phys. **13**, 936–941 (1986).

[31] M. B. Podgorsak, S. S. Kubsad, and B. R. Paliwal, ''Dosimetry of large wedged high-energy photon beams,'' Med. Phys. **20**, 369–373 (1993).

[32] M. K. Woo, A. Fung, and P. O'Brien, ''Treatment planning for asymmetric jaws on a commercial TP system,'' Med. Phys. **19**, 1273–1275 (1992).

[33] J. R. Palta, K. M. Ayyangar, and N. Suntharalingam, ''Dosimetric characteristics of a 6 MV photon beam from a linear accelerator with asymmetric collimator jaws,'' Int. J. Radiat. Oncol., Biol., Phys. **14**, 383–387 (1988).

[34] M. K. Yu, S. R. Sloboda, and B. Murray, ''Linear accelerator photon beam quality at off-axis points,'' Med. Phys. **24**, 233–239 (1997).

[35] R. C. Tailor, V. M. Tello, C. B. Schroy, M. Vossler, and W. F. Hanson, ''A generic off-axis energy correction for linac photon beam dosimetry,'' Med. Phys. **25**, 662–667 (1998).

[36] J. A. Purdy, W. Harms, W. F. Hanson, P. Kennedy, T. Kirby, A. Niroomand-Rad, and J. R. Palta, AAPM RTC TG-46: X-ray Beam Central Axis Depth-Dose Data for Use in Radiation Therapy, Med. Phys. [1997 (draft approved by Radiation Therapy Committee)].

[37] J. R. Palta, K. Ayyangar, I. Daftari, and N. Suntharalingam, ''Characteristics of photon beams from Philips SL25 linear accelerators,'' Med. Phys. **17**, 106–116 (1990).

[38] J. H. Hubbell and S. M. Seltzer, Tables of X-Ray Mass Attenuation Co-

efficients and Mass Energy-Absorption Coefficients 1 keV to 20 MeV for Elements $Z=1$ to 92 and 48 Additional Substances of Dosimetric Interest, Technical Report NISTIR 5632, NIST, Gaithersburg, MD, 1995.

[39] D. W. O. Rogers, C. M. Ma, G. X. Ding, B. Walters, D. Sheikh-Bagheri, and G. G. Zhang, BEAM98 Users Manual, NRC Report PIRS 509(a)revC (1998).

[40] G. Marsaglia and A. Zaman, ''A new class of random number generators,'' Annals Appl. Probability **1**, 462–480 (1991).

[41] M. K. Fix, M. Stampanoni, P. Manser, E. J. Born, R. Mini, and P. Rüegsegger, ''A multiple source model for 6 MV photon beam dose calculations using Monte Carlo,'' Phys. Med. Biol. **46**, 1407–1427 (2001).